ANNALS OF GEOPHYSICS, 69, 5, A552, 2026; doi:10.4401/ag-9533
OPEN ACCESS

Asymmetric patterns of ENSO phases in Indonesia between 1975-2025 and corresponding impacts on rainfall variability

Endah Rahmawati[*,1], Tjipto Prastowo[1]

(1) The State University of Surabaya, Physics Department, Surabaya, Indonesia

Article history: received January 15, 2026; accepted July 22, 2026

Abstract

El Niño-Southern Oscillation (ENSO) is a climate phenomenon affected by anomalies in sea surface temperature in the central-eastern Pacific and atmospheric pressure difference between Tahiti and Darwin. Such anomalies are called Oceanic Niño Index (ONI) and Southern Oscillation Index (SOI). In this study, we used these indices to examine the behaviours of El Niño and La Niña in Indonesia between 1975-2025 focusing on periodicity and strength, and the impacts of ENSO asymmetry on rainfall patterns. The methods included the Pearson and lagged analyses to quantify correlations between climate variables. Fast Fourier Transform (FFT) and wavelet techniques were also used to determine the recurrent intervals of El Niño and La Niña. The results showed that the indices are well-corresponded in Niño 3.4 and have a strong correlation of –0.76. It suggests that both are good indicators, correlated with rainfall anomaly at only moderate modes of –0.63 and 0.59 respectively, with $p \leq 0.001$, confirming statistical significance between the indices and rainfall variations. Strong impacts of El Niño occurred in June-July-August (JJA) and September-October-November (SON), where rainfall deficits led El Niño by 3 months before its peak in November-December-January (NDJ). The FFT analysis and wavelets revealed asymmetric patterns of the ENSO phases, where the recurrent intervals of El Niño and La Niña were respectively found to be 3.7-5.2 years and 2.7-3.8 years, classified into the short-term interannual variations, with El Niño's peaks attain a significantly larger intensity than those of La Niña. The FFT and wavelets showed secondary oscillation at time-scales longer than 10 years, indicating the long-term decadal variations hence the non-stationary (time-dependent) nature of ENSO variability. These suggest that strong El Niño tends to be more intense, leading to drier atmospheric conditions while strong La Niña occurs more frequently, indicating possible extreme weather for Indonesia in the future.

Keywords: ENSO; El Niño; La Niña; ONI; SOI; Asymmetric Patterns; Extreme Weather

1. Introduction

The Indo-equatorial Pacific region is part of the world climate system, a key regulator for climate variability at regional and global scales. Indeed, it is in this region in which El Niño-Southern Oscillation (ENSO), a complex

natural phenomenon, takes place under controlled by regional air-sea circulation near and in the tropical Pacific but can have significant effects on far-reaching regions from the tropics (McPhaden, 2015; Sullivan et al., 2016; Paek et al., 2017; Timmermann et al., 2018; McPhaden et al., 2020; Santoso et al., 2022; Li et al., 2023). Generally, the ENSO fluctuates at interannual time-scales (Sullivan et al., 2016; Timmermann et al., 2018; Le and Bae, 2019; Glantz and Ramirez, 2020; Iwakiri and Watanabe, 2021; Liu et al., 2022; Freund et al., 2024) between the neutral, El Niño, and La Niña phases, where the last two are widely known as opposing phenomena, only to occur when specific conditions on atmosperic and oceanic parameters are fulfilled.

When the equatorial Pacific is in normal conditions, it is said to be in the neutral phase. A measured shift in these conditions in the eastern tropical Pacific leads to the warm (cold) phase of the ENSO, called El Niño (La Niña) (Geng et al., 2019; Chen et al., 2021; Li et al., 2023; Ehsan et al., 2024). When the easterlies (blowing from east to west) along the equator are weakening, the flow of warmer surface waters towards the western Pacific is reduced, resulting in a cool state of the western Pacific waters and a warm state of the eastern Pacific waters. This condition is called El Niño. In terms of sea surface temperature (SST) and sea level pressure (SLP), El Niño episodes are characterised by warmer than average SST in the central and eastern tropical Pacific and higher SLP in the western Pacific (Sayol et al., 2022; Torres et al., 2023; Parra et al., 2024). The opposite condition occurs when the easterlies are strengthening, the flux of warmer waters towards the western Pacific is increased, leading to a warm state of the western Pacific and a cool state of the eastern Pacific. This condition is called La Niña. A long-term statistical analysis (Jia et al., 2025) has recently revealed that El Niño episodes tend to be more intense whereas La Niña episodes last longer and occur more frequently, making ENSO variability uniquely asymmetric (Geng et al., 2019; McPhaden et al., 2020; Chen et al., 2021; Fan et al., 2023; Jia et al., 2025).

A number of previous studies dating back to early work on the Southern Oscillation in relation to changes in SST variations over the equatorial Pacific (Walker, 1928; Bjerknes, 1969; Julian and Chervin, 1978) and recent publications (Timmermann et al., 2018; Geng et al., 2019; McPhaden et al., 2020; Freund et al., 2024) have claimed that the Southern Oscillation is an atmopsheric component of the ENSO, intimately connected to changes in oceanic parameters. It is also known as the oscillatory exchange of atmospheric masses between connected regions in the eastern South Pacific and Indonesia at interannual time-scales. This strong atmosphere-ocean interaction centred in the equatorial Pacific can influence weather and climate patterns in other parts of the globe through atmospheric teleconnections (Bjerknes, 1969) by which regions that are remote from the Pacific, such as North and South America (Feldstein and Franzke, 2017; Kayano et al., 2021) and North Atlantic-Europe (Ayarzagüena et al., 2018; Molteni and Brookshaw, 2023) can be affected by global circulation of clouds and precipitation. Therefore, ENSO variability has significant, far-reaching effects on weather and climate worldwide.

During El Niño episodes, atmospheric pressure over Indonesia and the northern Australia in the western Pacific is anomalously high and the pressure over the eastern Pacific is relatively low. It follows that atmospheric-oceanic conditions characterising El Niño episodes are high air pressure in Darwin over cold waters in the western Pacific, accompanied by low air pressure in Tahiti over warm waters in the central and eastern Pacific. It is then easy to understand that a reverse situation in the oscillation takes place during La Niña episodes.

In the tropical Pacific, routine ocean surface monitoring of SST and SLP anomalies are reported as Oceanic Niño Index (ONI) and Southern Oscillation Index (SOI), respectively. The ONI is a measure of the strength of an El Niño (La Niña) event based on SST anomaly (SSTA) measurements, exceeding a threshold (measured in degree Celcius) in the Niño 3.4 region. The commonly used threshold ONI to indicate El Niño (La Niña) for the warm (cold) phase of the ENSO is a positive (negative) SST departure, deviating from average equal to or greater (lower) than +0.5°C (−0.5°C) to be obtained for five consecutive 3-month running mean SSTA. The SOI is a measure of the strength of the Southern Oscillation, calculated from variations in air pressure difference between Tahiti in the south-central Pacific and Darwin in the south-western Pacific. While a positive (negative) ONI relates to El Niño (La Niña), reverse conventions are taken, where a negative (positive) SOI refers to El Niño (La Niña), associated with the warm (cold) phase of the ENSO (see https://www.ncei.noaa.gov/access/monitoring/enso/soi for details).

During El Niño (La Niña) episodes, there is less (frequent) rainfall and drier (wetter) atmospheric conditions, widespreading in Indonesian territory (Aldrian and Susanto, 2003; Aldrian et al., 2007; Lee, 2015). Hence, ENSO events relate to a significant increase or decrease in the frequency and severity of hydrometeorological hazards, such as extreme droughts and floods. A number of studies on rainfall variability over Indonesia and its close linkage with the large-scale climatic ENSO phenomenon were well-documented (Kirono et al., 1999; Hamada et al., 2002; Aldrian and Susanto, 2003; Hendon, 2003; Aldrian et al., 2007; Lee, 2015; Hidayat, 2016; Lestari et al., 2018; Amirudin et al., 2020; Kurniadi et al., 2021; Ratri et al., 2021; Ariska et al., 2024). However, these studies did not consider the impacts

of El Niño or La Niña on mean precipitation rates under the influence of ENSO asymmetry in periodicity and intensity (a factor being not yet discussed). Using the ONI and SOI time-series between 1975-2025 (sufficiently long duration of observation), we analyse the relative importance of El Niño and La Niña in association with ENSO asymmetric behaviours and the resulting impacts on the rainfall variability.

The aims of this study are twofold. Firstly, we use the ENSO indices (ONI and SOI) to examine the behaviours of El Niño and La Niña in Indonesia between 1975-2025, focusing on their periodicity and intensity using SSTA measurements from the Niño 3.4 in the tropical Pacific, bordered by 5°N-5°S and 120°W-170°W (see Fig. 1) and SLP gradients between Tahiti and Darwin. El Niño (La Niña) episodes are to take place when SSTA in the Niño 3.4 ≥ 0.5°C that are lasting for several months in two consecutive years. Secondly, as Indonesia is a country dependent on agriculture and fishing for livelihood, which is likely affected by the ENSO, we also examine the effects of ENSO asymmetry on rainfall patterns. Given the frequency and intensity of anomalous climate conditions in Indonesia, resulting in extreme dry (wet) atmospheric conditions that may lead to severe droughts (floods), full knowledge of the ENSO variability and its impacts on rainfall is useful for building capacity towards enhanced societal readiness (Glantz and Ramirez, 2020). This becomes part of anticipation and hence community-based national resilience to climate-related hazards, considering worsening impacts of the ENSO in the future (Glantz and Ramirez, 2025).

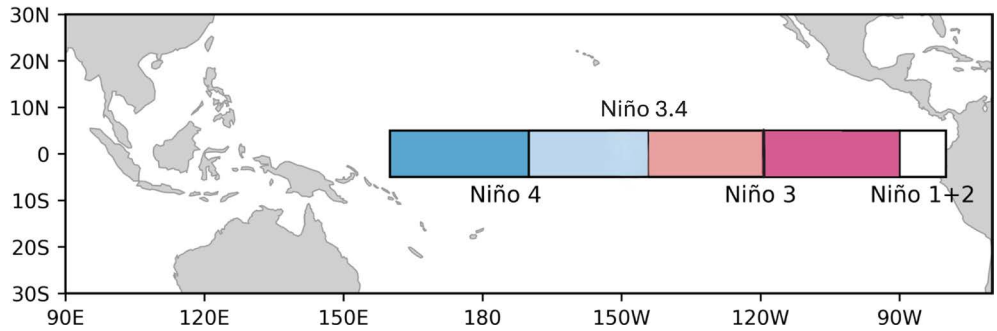

Figure 1. Illustration of ocean surface monitoring in the eastern and central tropical Pacific, where the Niño 3.4 spans from 120°W to 170°W longitude and 5°N to 5°S latitude. The ONI is obtained from measurements of SST anomalies (averaged over a 3-month running period).

This study is considered more comprehensive than earlier work of Ratri et al. (2021), involving a specific region of interest within the country (i.e., Java Island, widely known as the centre for agriculture and food production) or other studies, discussing a single El Niño and its corresponding impacts on rainfall at a nationwide scale, such as fatal drought in the 1997/98 (Kirono et al., 1999) and the 2015/16 cases (Lestari et al., 2018). Amirudin et al. (2020) and Kurniadi et al. (2021) examined impacts of the Pacific-Indian interaction on Indonesian rainfall patterns but they did not evaluate effects of ENSO asymmetry on rainfall variability. Ariska et al. (2024) studied Indonesian rainfall in connection to the linked tropical Pacific-Indian Ocean using rainfall data, spanning between 1981-2016. Past studies working on the ENSO-rainfall anomaly relationship over Indonesia (Hamada et al., 2002; Hendon, 2003) employed different spanning data from 1961-1990 and 1951-1997, respectively, but remaining shorter than a period of 1975-2025 used in this work. More importantly, these data did not include 3 severe El Niño events in 1982/83, 1997/98, and 2015/16 for comparison. Indeed, this study emphasises how close ENSO asymmetry is connected to the large-scale rainfall anomalies across the country during a longer time-interval of observation.

2. Methodology

2.1 Parameters and ONI data sources

The ONI, an internationally standardised index of SSTA measurements, is made possible by National Centers for Environmental Prediction (NCEP), National Oceanic and Atmospheric Administration (NOAA), US to identify El Niño (warm) and La Niña (cool) phases of the climatic ENSO conditions in the central-eastern tropical Pacific.

It is the running 3-month mean SSTA in the Niño 3.4 region (see Fig. 1). This region is essential for measurements of SSTA as it encompasses the western half of the equatorial cold tongue, providing a good measure of changes in SST that in turn lead to variations in patterns of regional tropical convection and atmospheric circulation.

The term of El Niño or La Niña is defined as five consecutive overlapping 3-month periods to be equal to or greater than the common value SSTA of +0.5°C for El Niño and equal to or lower than the common value SSTA of −0.5°C for La Niña. Modified from https://ggweather.com/enso/oni.htm, thresholds for El Niño modes are divided into weak (SSTA from 0.5 to 0.9), moderate (SSTA from 1.0 to 1.4), strong (SSTA from 1.5 to 1.9), very strong (SSTA from 2.0 to 2.4), and extreme (SSTA ≥ 2.5). The thresholds for La Niña modes are similar but in negative numbers. ENSO years (classified into their strength) are then provided in Table 1 for completeness.

Table 1. Modes of El Niño and La Niña years during 1975-2025 based on ONI measurements in the Niño 3.4 region.

El Niño					La Niña		
Weak	Moderate	Strong	Very Strong	Extreme	Weak	Moderate	Strong
1976/77	1986/87	1987/88	1982/83	2015/16	1974/75	1995/96	1975/76
1977/78	1994/95	1991/92	1997/98		1983/84	2011/12	1988/89
1979/80	2002/03	2023/24			1984/85	2020/21	1998/99
2004/05	2009/10				2000/01	2021/22	1999/00
2006/07					2005/06		2007/08
2014/15					2008/09		2010/11
2018/19					2016/17		
2019/20					2017/18		
					2022/23		
					2024/25		

The ONI at https://www.cpc.ncep.noaa.gov/products/analysis_monitoring/ensostuff/detrend.nino34.ascii.txt were measured in the Niño 3.4, freely available in months from January to December during observational years. Monthly ONI data are known to be inherently noisy because randomness, where short-term atmospheric shifts may change SST. Thus, we used overlapping seasons for ONI data, referring to the 3-month running mean SSTA, such as August-September-October (ASO), September-October-November (SON), October-November-December (OND) to identify a correct ENSO phase: the warm (El Niño) or the cold (La Niña) episode. Using the overlapping seasonal data, we may define the life-cycle of a single El Niño or La Niña event, which usually peaks during NDJ. The seasonal data were freely accessible at https://www.cpc.ncep.noaa.gov/data/indices/oni.ascii.txt. For example, the data from December 1979 to February 1980 were abbreviated as DJF 1980 and those from November 1980 to January 1981 were called NDJ 1980. These were provided using the NOAA Extended Reconstructed Sea Surface Temperature version 5 (ERSSTv5) (see Huang et al., 2017 for all further detailed upgrades, validations, and intercomparisons). The ERSSTv5 provides the spatially-complete, global data of SSTA directly acquired from routine monitoring of the ocean surface worldwide.

2.2 Parameters and SOI data sources

The Southern Oscillation reflects variations in the SLP difference between monitoring stations at Tahiti in the central south Pacific and Darwin in the northern Australia, quantified as the SOI. Thus, the SOI is an internationally standardised index of measurements between two barometric pressures, namely SLP difference and SLP difference anomaly between these regions. In normal conditions, low pressure over Darwin and relatively higher pressure over Tahiti drive a circulation of air from east to west across the Pacific, drawing warm surface water westward and bringing precipitation to Australia and the western Pacific. The SOI values are made by NCEP, NOAA to differ El Niño from La Niña, accessible for free at https://www.cpc.ncep.noaa.gov/data/indices/soi.3m.txt where the data are available in months on the basis of the 3-month running mean pressure anomaly measurements. The methodology used to calculate the SOI is provided below,

$$\mathrm{SOI} = \frac{s\mathrm{SLP}_{\mathrm{Tahiti}} - s\mathrm{SLP}_{\mathrm{Darwin}}}{\sigma_{\mathrm{monthly}}} \tag{1}$$

where $s\mathrm{SLP}_{\mathrm{Tahiti}}$ and $s\mathrm{SLP}_{\mathrm{Darwin}}$ are both standardised SLP measured in Tahiti and Darwin, respectively, and

$$\sigma_{\mathrm{monthly}} = \sqrt{\frac{\sum(s\mathrm{SLP}_{\mathrm{Tahiti}} - s\mathrm{SLP}_{\mathrm{Darwin}})^2}{N}} \tag{2}$$

where N is the number of months. The standardised SLP for each in Eq. (2) is given by

$$s\mathrm{SLP} = \frac{a\mathrm{SLP} - m\mathrm{SLP}}{\sigma} \tag{3}$$

where aSLP and mSLP are the actual and mean SLPs, respectively, and the denominator σ represents standard deviation given by

$$\sigma = \sqrt{\frac{\sum(a\mathrm{SLP} - m\mathrm{SLP})^2}{N}} \tag{4}$$

2.3 Data sources of Indonesian rainfall variability

Historical data for Indonesian rainfall variability (presented as annual precipitation) are derived from Climatic Research Unit (CRU), University of East Anglia, UK where time-series data (CRU-TS) version 4.08 gridded datasets are presented using a $0.5^{\circ} \times 0.5^{\circ}$ (50 km × 50 km) resolution and available between 1901-2024. These datasets were obtained for free from https://climateknowledgeportal.worldbank.org/country/indonesia/climate-data-historical (operated for land-based observations). The World Bank Group (WBG) has supported Climate Change Knowledge Portal (CCKP) data for promoting Climate Risk Country Profiles (CRCP), high-level assessment of climate risks for developing countries worldwide (see https://climateknowledgeportal.worldbank.org/country-profiles for further details). Knowledge of these potential risks is used to develop a better understanding of current climatic conditions and accommodate future climate projections for a country or a region of interest under particular climate scenarios in the context of minimising climate-related hazards.

When performing time-series analysis of ENSO indices and Indonesian rainfall anomalies, all the time-series are required to be presented using the same time-interval. As historical data for Indonesian rainfall anomalies by the worldbank portal (see the above hyperlink) are given in the form of annual precipitation, we therefore selected Indonesian monthly rainfall from https://crudata.uea.ac.uk/cru/data/hrg/ in the observational years of 1975-2024. This source provides high-resolution datasets of CRU-TS 4.09, the latest version of rainfall data around the globe to date. We performed simple statistical tests using rainfall data from both sources and found that the two versions

are very strong correlated and considered statistically significant. Thus, there is no significant bias in the results when either version of CRU time-series is used for cross-correlation calculations.

2.4 Statistical approaches

2.4.1 Pearson correlation analysis

In climate studies, cross-correlation analysis is commonly used to determine a relationship between a pair of climate variables tested that are continuous, independent, and normally distributed with no outliers. In this study, a linear Pearson correlation analysis was used to quantify a correlation coefficient r, representing the strength and direction of a relationship between the ENSO indices and rainfall anomalies. The Pearson correlation coefficient is calculated from

$$r = \frac{n\sum xy - (\sum x)(\sum y)}{\sqrt{(n(\sum x^2) - (\sum x)^2)(n(\sum y^2) - (\sum y)^2)}} \tag{5}$$

where n is the number of pairs of climate data, and x and y are the variables. The paired variables are as follows: (a) ONI-SOI; (b) ONI-anomalous rainfall; and (c) SOI-anomalous rainfall.

It is understood that Eq. (5) leads to $-1 \leq r \leq 1$. No correlation between the variables is associated with $r = 0$. A perfect positive correlation corresponds to $r = 1$; as one variable increases, the other also increases (changes in the same direction). A perfect negative correlation is satisfied when $r = -1$; as one variable increases, the other decreases (changes in the opposite direction). In most cases, the strength of the relationship between the variables is such that r falls within −1 and 1. We here adopted a conventional approach to interpret a correlation coefficient (see Schober et al., 2018) given by its magnitude as follows: negligible for $0 \leq r \leq 0.10$; weak for $0.11 \leq r \leq 0.39$; moderate for $0.40 \leq r \leq 0.69$; strong for $0.70 \leq r \leq 0.89$; and very strong for $0.90 \leq r \leq 1$.

2.4.2 Significance testing

To test whether variations of ENSO indices (ONI and SOI) and rainfall intensities during observational years are statistically significant, a statistical significance test was applied. This test resulted in a p-value, a measure of the probability of obtaining the observed results, assuming that the null hypothesis (a prediction of no relationship or no statistical significance between the variables) is true (see Greenland et al., 2016). The smaller the p-value, the greater the statistical significance between the variables. Thus, we can say that a p-value of 0.05 or smaller is considered statistically significant (the null hypothesis is rejected). However, in climate data even a small p-value is not necessarily proof of statistical significance as there remains a possibility that the data are obtained by chance. Only data of large size can confirm if a relationship between variables is statistically significant.

2.4.3 Time-lag correlation analysis

In addition to the Pearson correlation analysis, a time-lag correlation analysis was also performed to evaluate the relationship between the paired time-series (the ENSO indices and precipitation rates). This was completed by shifting one particular time-series forward or backward in time relative to the other. In this study, ONI time series (or alternatively, SOI time series) was shifted forward in time relative to rainfall anomaly time-series. Therefore, a lagged correlation coefficient $r(k)$ between ONI and rainfall data is calculated from

$$r(k) = \mathrm{Corr}(\mathrm{ONI}_{t-k}, R_t) \tag{6}$$

where R represents rainfall anomaly, t is an integer ($t = 0, 1, 2, \ldots$), and k is such that $r(k)$ reaches optimum. Following the work of Setyaningrum et al. (2026), when $k > 0$, atmospheric response leading to rainfall anomalies

follow changes in SST or lag behind ONI values. When $k < 0$, the anomalies take place prior to the significantly altered ONI, representing the corresponding oceanic shift in SST in the Pacific (assuming that surface temperature changes in the Pacific is the only trigger for rainfal patterns). When $k = 0$, this leads to the Pearson correlation of no lags or no leads between the variables.

The goal of this approach was to determine delayed effects and the optimum solution to the time delay (if any) between the paired variables selected that results in the strongest correlation. The lagged analysis can thus be used to describe whether there is a delayed atmospheric response of precipitation observed as anomalous rainfall to ENSO forcings represented by the ONI and SOI time-series. Knowledge of this time-lag helps determine the precise interval between a trigger ENSO event (if a delayed atmospheric response is present) and its resulting impacts on the Indonesian rainfall anomaly.

2.5 Time-frequency methods

2.5.1 Spectral analysis of ONI and SOI time-series

Rather than taking a single time-range of a primary period of ENSO oscillations, for example, between 3-8 years (Okumura and Deser, 2010), we used the Fast Fourier Transform (FFT) as a tool for a conversion of an ENSO signal given in the time-domain (either the ONI or SOI time-series) into individual spectral components to determine recurrent intervals of El Niño and La Niña episodes separately. These components provide frequency distribution of the signal, with which the dominant periods of the time-series were then identified. It follows that any waveform of time-domain can be decomposed into a sum of varying sinusoidal oscillations at different frequencies, for which this method is frequently called time-frequency analysis of the ENSO. Each oscillation has its own amplitude and phase, from which the power spectral density was derived to reveal the variance in the spectral at different periods. This approach was motivated by observations that the behaviours of El Niño and La Niña represented by the ONI and SOI time-series are likely periodic. This knowledge was used to determine periodic components embedded in the time-series by calculating the associated periods, amplitudes, and phases.

In short, using the optimum solution to power spectrum estimation we can determine the dominant periods of the signal. Therefore, as pointed out by Ghil et al. (2002), the strength of the time-frequency analysis is to provide a theoretical framework for diagnosing climate variability indicated by temporal variations of ENSO indices and the associated anomalous rainfall in a region of interest by highlighting recurrent spectral ENSO phases separately. The FFT can be written in a discrete form (see Crockett, 2019) as follows,

$$F_m = \frac{1}{N}\sum_{n=0}^{n=N-1} f_n \exp\left(\frac{-i2\pi mn}{N}\right) \tag{7}$$

where F_m is a function in the frequency-domain, f_n is a function in the time-domain, and n and m are integer numbers in the time- and frequency-domain signals, respectively.

2.5.2 Wavelet analysis

Wavelet analysis decomposes complex ENSO signals into time-frequency domain, pinning the dominant cycles of the ENSO and showing the shift in the intensity at their peaks over time. Unlike the traditional Fourier analysis, this technique deals with the non-stationary nature of ENSO variability, making it the primary tool for examining its time evolution. In this sense, it is used to measure how strong localised time-frequency correlations are between the observed signals, allowing us to identify not only whether the signals are correlated but during which time and at what scales the correlations take place. Contrary to the FFT, wavelets may detect either short-term (interannual) or long-term (decadal) fluctuations of the ENSO cycles in driving the correlations, thereby supporting evidence for time-varying ENSO periodicity and multi periods of ENSO (see Tamaddun et al., 2017). Hence, the advantage of wavelets is concerned with ENSO intermittent peaks and non-linearity in the power spectrum that may not be concidered by a standard linear analysis of signal processing.

3. Results and Discussions

3.1 Correlations between ONI, SOI, and rainfall data

There are 4 regions spanning from the eastern to the western tropical Pacific, namely Niño 1+2, Niño 3, Niño 4, and Niño 3.4 encompassing parts of Niño 3 and Niño 4 (see Fig. 1), where SST anomalies (averaged across a given region) are monitored by the ONI. Since many scientists (see, for example, from early work of Barnston et al. (1997) and Bunge and Clark (2009) to a recent publication by L'Heureux et al. (2024)) have learned from past ENSO studies, they agree with Niño 3.4 to be a key region for the study of ocean-atmosphere interaction along the tropical Pacific. Thus, the Niño 3.4 region becomes a favour for monitoring ocean surface temperature to examine the behaviours of El Niño and La Niña. While other regions are, on specific purpose, also used to characterise the ENSO phases (Sayol et al., 2022; Torres et al., 2023; Li et al., 2024), this study uses SST and SSTA measurements in the Niño 3.4 for examining ENSO asymmetric patterns and corresponding consequences for local to regional climate, such as rainfall variability over Indonesian territory during a given observation time.

As earlier pointed out, the ONI is not the only index to parameterise the warm and cold ENSO phases. Indeed, the SOI is also used to detect ENSO arrivals. These indices have to be self-consistent in the sense that they indicate the same occurrence of a particular ENSO phase (El Niño or La Niña) at the same time. For this reason, we provide smoothed time-series of the ONI in the Niño 3.4 region in Fig. 2a and the corresponding SOI smoothed time-series in Fig. 2b. The two time-series are presented to show how well they are correllated during the observations.

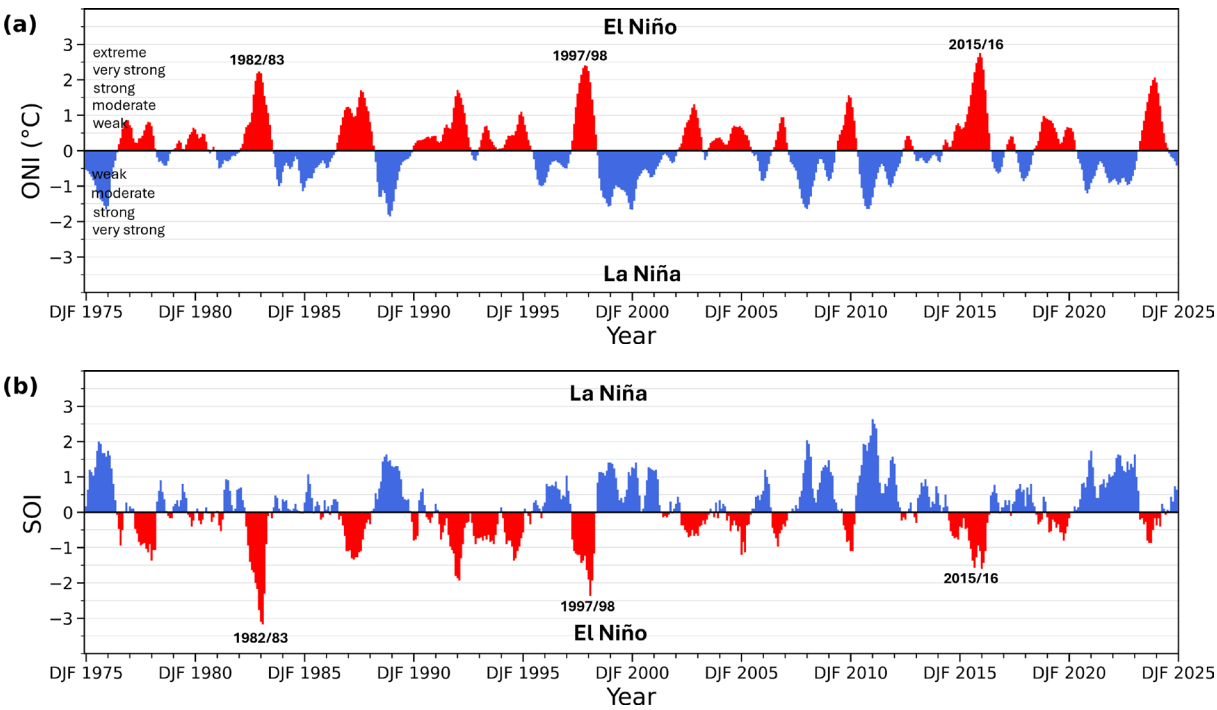

Figure 2. (a) Prolonged periods of measurements of the ONI and (b) similar measurements of the SOI between 1975-2025, showing some consistency in the ENSO indices during the observations.

Using positive ONI values (red in Fig. 2a) and negative SOI values (red in Fig. 2b) for El Niño, it is easy to justify that both indices showed very strong modes of El Niño in 1982/83 and 1997/98 with the ONI were between 2.0-2.4 and an extreme mode in 2015/16 with the ONI was measured to be greater than 2.5. Further, using negative ONI values (blue in Fig. 2a) and positive SOI values (blue in Fig. 2b) for La Niña, we found strong modes of La Niña in 1988/89, 1999/2000, 2007/08, and 2010/11 with the ONI fell within −1.5 to −1.9 and a moderate level of a triple-dip La Niña during 2020/21, 2021/22, and 2022/23 with the ONI was in the range −1.0 to −1.4. We can say that self-consistent performance of the ONI and SOI as the ENSO indicators (see Masood et al., 2023) is thus achieved during the observations. The ONI and SOI are strongly correlated, respectively representing the oceanic and atmospheric parts

of the large-scale ENSO climate phenomenon (see Santos et al., 2024). Although the SOI is less reliable than the ONI over long periods due to relatively high-frequency atmospheric noise, specific geographical positions of SOI monitoring stations, and no universal thresholds of the SOI for signaling ENSO arrivals, as opposed to the ONI, the indices are self-consistent for predicting an El Niño or La Niña event.

To support visual inspection showing the consistency between the ONI and the SOI seen in Fig. 2, we perform a quantitative assessment of an ONI-SOI relationship using the Pearson correlation coefficient r defined in Eq. (5). We also compute correlation coefficients between the ONI (SOI) and Indonesian rainfall anomaly. We then provide all the results in Table 2 and the corresponding scatters in Fig. 3.

Table 2. Correlations between seasonal ONI-SOI and rainfall anomaly during 1975-2024.

Season	Pearson correlation coefficient r		
	ONI-SOI	ONI-rainfall	SOI-rainfall
overall	−0.761	−0.626	0.585
DJF	−0.812	−0.483	0.496
MAM	−0.772	−0.370	0.331
JJA	−0.720	−0.758	0.688
SON	−0.737	−0.800	0.818

The calculations are placed in the light of recent ENSO studies (Amiruddin et al., 2020; Kurniadi et al., 2021; Ariska et al., 2024). They argued that the ONI and SOI reflect ENSO-related climate variability, particularly at interannual time-scales, and affect rainfall patterns across Indonesian regions. During their observations, rainfall patterns over Indonesia are found to strongly depend on season. It implies the relative importance of examining the effects of ENSO variability on the observed rainfall anomalies during independent 3-consecutive month periods (non-overlapping seasons) appropriate for Indonesian climate, namely: (1) December-February (DJF = wet season); (2) March-May (MAM = seasonal transition); (3) June-August (JJA = dry season); and (4) September-November (SON = seasonal transition).

Depicted in Fig. 3, the corresponding scatter-plots for all the linear Pearson correlations with a total of 201 data sampled from overall non-overlapping seasons given in Table 2.

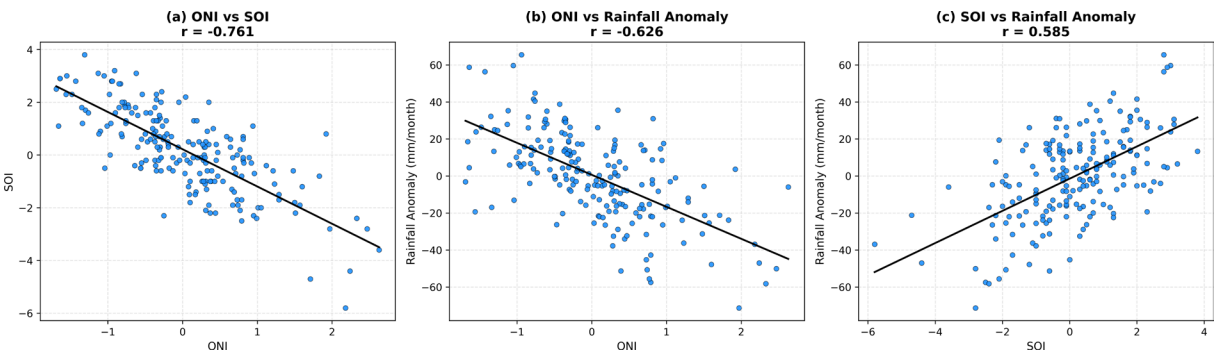

Figure 3. Scatters of (a) the ONI-SOI, (b) ONI-anomalous rainfall, and (c) SOI-anomalous rainfall relationships using all the data from the observational years, showing a strong correlation of ONI-SOI with $r = -0.76$ and moderate correlations between ONI-rainfall anomaly and SOI-rainfall anomaly with $r = -0.63$ and 0.59, respectively.

All the calculated coefficients seen in Table 2 are obtained with p-values below a cut-off of 0.05, indicating statistical significance of ONI to SOI and ONI or SOI to rainfall variations with a 95% probability of confidence (see Greenland et al., 2016). It suggests the plausible effects of one variable on another in the relationships. The strong correlation of ONI-SOI with the Pearson correlation coefficient $r \leq -0.72$ (rounded to two decimal places), falling within the same strong mode as that found by Kurniadi et al. (2021) for any season confirms that both ENSO indices serve as good indicators for El Niño or La Niña episodes. Seasonal rainfall over Indonesia is found to be moderately modified by the ENSO variability (−0.63 and 0.59 for ONI- and SOI-rainfall anomaly relationships, respectively), where the strong impacts on the rainfall anomalies occur during JJA and SON, consistent with previous work either using Indonesian climatic rainfall regions (Aldrian and Susanto, 2003; Aldrian et al., 2007; Kurniadi et al., 2021) or with no regional rainfall divisions (Kirono et al., 1999; Hamada et al., 2002; Hendon, 2003; Amiruddin et al., 2020) and the weaker impacts occur during DJF and MAM. In short, Indonesian rainfall patterns are widely influenced throughout the country by the ENSO variability with the strong (weak) impacts occur during the dry (wet) season and its associated seasonal transition.

Although the Pearson correlation analysis reveals how close the ONI, SOI, and seasonal rainfall anomaly are correlated one to another, it provides no information about whether there is a lagged or a leading relationship between two time series used in the paired climate variables. As argued by Hamada et al. (2002), changes in SST (represented by ONI values) influence local to regional atmospheric response, causing the onset of the wet season over Indonesian territory to come later (earlier) in El Niño (La Niña) years than usual. They further concluded that regional patterns of rainfall anomaly tend to appear earlier in the western regions than in the eastern, attributable to possible multiple triggers for temporal variations of Indonesian rainfall (the ENSO is likely not the only source affecting Indonesian rainfall).

As also suggested by other ENSO-Indonesian rainfall studies (Hendon, 2003; Lee, 2015; Amiruddin et al., 2020; Kurniadi et al., 2021; Ariska et al., 2024), possible interactions of ENSO and SST gradients between the western and eastern regions of the equatorial Indian Ocean that may influence rainfall variability over Indonesia must be considered (but this topic goes beyond the scope of this study). For this reason, the lagged correlation analysis is alternatively used to determine whether there is a delayed atmospheric response (observed as anomalous rainfall) to oceanic forcings. This time-lag analysis estimates how one dataset shifts in time (relative to the other) to achieve the strongest correlation between the variables, confirming which variable comes earlier. It may also indicate that additional influential factors need to be taken into account for the observed rainfall anomalies.

The negative lags seen in Figs. 4b and 4c where the strongest correlations are achieved at $k = -3$ indicate that changes in rainfall with significantly low (high) rainfall intensity measured over Indonesia appear to observe before the corresponding shift detected as the increased (decreased) ONI values in the Niño 3.4 during the dry (wet) season of JJA (DJF) and SON (MAM) in El Niño (La Niña) years. This is consistent with previous work (Hamada et al., 2002; Kurniadi et al., 2021) but none of these studies reported the precise lag of 3 months between the altered rainfall and the oceanic index (ONI). The lag reflects that the large-scale SSTA in the tropical Pacific is not the only trigger for rainfall anomaly. Instead, it is also likely driven by additional influential factors other than the ENSO, such as the Indian Ocean Dipole (IOD) and local seas surrounding islands in Indonesian archipelago.

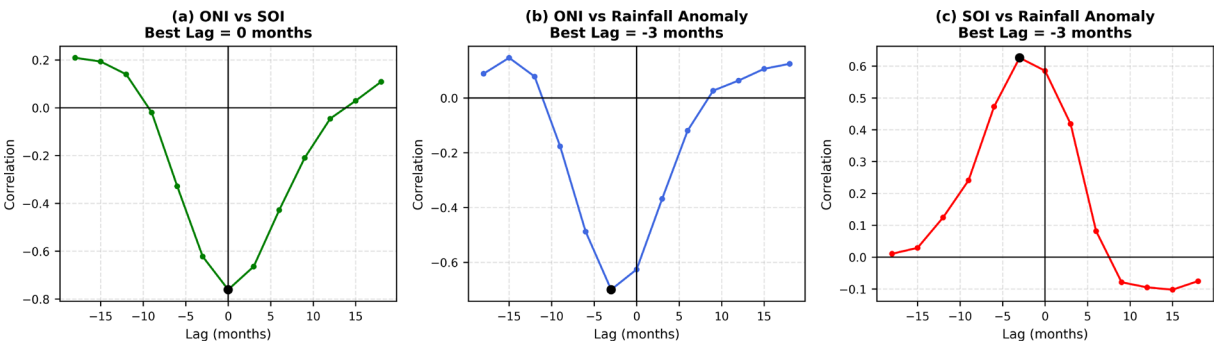

Figure 4. The lagged correlations of (a) ONI-SOI, (b) ONI-anomalous rainfall, and (c) SOI-anomalous rainfall calculated from Eq. (6), where $k = 0$ in (a) representing no lag between the ONI and SOI time series. The strongest correlations occur at $k = -3$ in (b) and (c), indicating that Indonesian rainfall anomalies emerge approximately 3 months before the ENSO indices reach their optimum values.

Identification of the negatif lags is essential. It allows the Indonesian government to do anticipatory action for extreme precipitation as part of nationwide preparedness for hydrometeorological hazards (Ariska et al., 2024). Rainfall extreme with very high or low intensity may lead to climate-related disasters, such as prolonged droughts and forest fires during extreme dry atmospheric conditions or severe floods, landslides, and soil erosion during extreme wet atmospheric conditions (Kurniadi et al., 2021). If rainfall anomalies remain persistently occurring before changes in SST towards a definitive ONI phase (an El Niño or La Niña event), the early rainfall can be used as a precursor to predict the arrival of El Niño or La Niña, as well as to estimate whether El Niño or La Niña is about to strengthen or weaken in upcoming months.

3.2 ENSO asymmetry in periodicity and intensity

It is clear from observational data that El Niño and La Niña are not perfectly opposing phenomena. These ENSO phases show apparently asymmetric behaviours in temporal evolution, duration, frequency of occurrence, and amplitude patterns (Geng et al., 2019; McPhaden et al., 2020; Chen et al., 2021; Jia et al., 2025; Liang et al., 2025). Whilst, in this study asymmetric patterns of the ENSO phases refer to differences in periodicity (time interval between two consecutive El Niño or La Niña events) and intensity. The following paragraphs discuss how the ONI and SOI time-series (see Fig. 2) and the corresponding FFT and wavelet analyses of the ONI (see Figs. 5 and 6) are used to obtain information on ENSO asymmetry in periodicity and intensity.

As stated, the ONI and SOI are both used to monitor the arrivals of the warm and cold ENSO phases (see Fig. 2). A total of 17 warm phases (El Niño) and 18 cold phases (La Niña) with 15 neutral phases in between were recorded between 1975-2025. Of 17 El Niños, 7 occurrences were considered weak, 3 events for each in moderate, strong, and very strong modes, and 1 event in an extreme level. Whilst, 18 La Niñas were divided into 8 weak, 4 moderate, and 6 strong modes. These classifications are consistent with previous studies (Cai et al., 2018; Geng et al., 2023; Wang et al., 2023) using various methods to define the ENSO amplitude and multi-year La Niña. The difference in event frequency between El Niño and La Niña reflects that La Niña tends to be more frequent to occur, suggesting a shorter period of La Niña than El Niño. During the observations, multi-year La Niña occurred twice between 1998-2000 and 2020-2022, showing a positive trend for La Niña to be persistent for multi years (Wang et al., 2023) following an apparent shift in ENSO dynamics after 1990 (Li et al., 2024). Conversely, no multi-year El Niño was recorded because El Niño events are short-lived and La Niña events last longer (due to its persistence), consistent with previous findings (Okumura and Deser, 2010; Choi et al., 2013; An and Kim, 2017; Geng et al., 2019).

What is missing in the preceeding paragraph is that it only provides description with no quantitative evaluation of the nature of ENSO variability. Time-frequency analysis is applied to the ONI and SOI time-series for comparison (but the analysis of the SOI is not reported here) using the FFT in Eq. (7) and wavelet techniques. This analysis was performed by converting ENSO signals in the time-domain into individual components in the frequency-domain to determine modes of ENSO oscillation. The resulting frequencies, periods, and power (representing intensities) are summarised in Table 3.

Table 3. Determination of modes of ENSO oscillation using the FFT applied to the ONI time-series.

Signal	Peak	Frequency (cycles/month)	Period (months)	Power	Time-scale
ENSO	1	0.0151	66.4444	2973.83	interannual
	2	0.0067	149.5000	2674.29	decadal
	3	0.0234	42.7143	1651.15	interannual
	4	0.0268	37.3750	395.10	interannual

Table 3 clearly reveals two distinct oscillation modes, namely interannual (short-term) and decadal (long-term). We argue for the work of Chen et al. (2024), who classified modes of ENSO oscillation into interannual fluctuation of 3-8 years and decadal variability of 10-16 years. In this study, the ENSO cycle is detected to vary in the range of 3.1-5.5 years, rounded to a decimal place from their corresponding periods in months, listed as Peaks 4 and 1 at interannual time-scales (see Table 3). This finding is aligned with the mainly interannual ENSO mode claimed by many climate studies (Le and Bae, 2019; Amirudin et al., 2020; Kurniadi et al., 2021; Liu et al., 2022; Li et al., 2023; Li et al., 2024; Liang et al., 2025). Independent oscillation of the ENSO is also observed with a significant intensity at a longer time-scale of about 12.5 years (seen as Peak 2 in Table 3 and Fig. 5), within the range of the long-term, slowly-varying oscillation referred to as decadal variability (Chen et al., 2024).

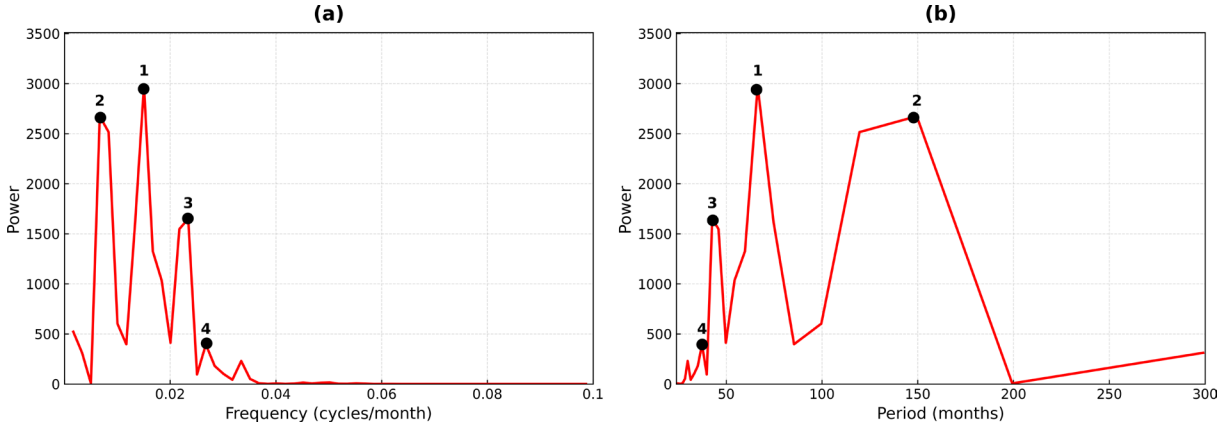

Figure 5. The results of the FFT analysis using the ONI, showing the nature of time-dependent ENSO modes with the resulting distribution of (a) frequencies and (b) corresponding periods.

While the FFT analysis reveals the short- and long-term fluctuations of the ENSO corresponding to interannual and decadal variabilities, respectively, the asymmetry in periodicity and intensity remains unresolved. To this end, we apply continuous wavelet transform (CWT) to the ONI datasets to resolve the problems in question and provide the results in Fig. 6.

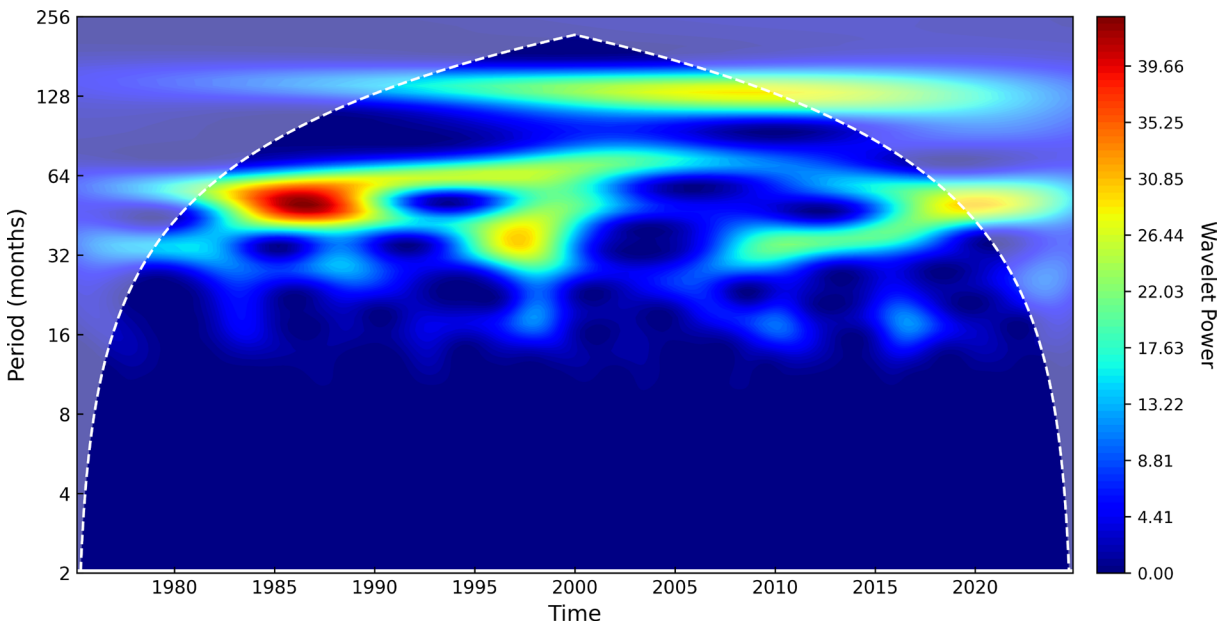

Figure 6. The results of the CWT on the ONI with the Cone of Influence (COI), a boundary on a time-frequency diagram that delineates regions affected by edge effects (see Krajl et al., 2024 for further details), is seen as a curved white dashed-line covering regions within which interpretation is believed to be true. The wavelet shows the nature of the ENSO patterns, which vary with time of observation (in years) and period of oscillation (in months).

Clearly seen in Fig. 6, a bright red-area indicates high intensity of the power spectral density, concentrated on a period of 44-62 months equivalent to 3.7-5.2 years between 1982-1988. During these years, 2 weak La Niña events in 1983/84 and 1984/85 followed by a neutral phase in 1985/86 were suppressed by the very strong 1982/83, moderate 1986/87, and strong 1987/88 El Niño episodes (see Table 1). As this feature dominates over other areas within the COI, temporal variability of the ENSO at time-scales of shorter than 96 months (classified into the short-term fluctuation) can be associated with El Niño periodic cycles. It suggests that the recurrent interval of El Niño is lying between 3.7-5.2 years, falling within the range of 3.1-5.5 years found for the main ENSO cycle (Table 3), consistent with recent studies (Chen et al., 2024; Liang et al., 2025). Other features with lesser power are also observed with a shorter period of 32-42 months, comparable to the periods of Peaks 3 and 4 given in Table 3, associated with the growth and development of the severe 1997/98 and 2015/16 El Niño events. A possible reason for a clear difference in intensity of the power spectral between the 1982/83 El Niño and the other two events may be related to different mechanisms of surface warming in the Pacific under recent global warming (Cai et al., 2018) that may lead to an apparent shift in ENSO patterns hence El Niño dynamics after 1990 (Li et al., 2024).

During 1999-2011, ENSO is observed to oscillate with moderate power at much lower frequencies and at periods longer than 96 months, considered to be decadal variability. Apparently stretched from 2007 to 2015, ENSO signals with a period of 32-45 months equivalent to 2.7-3.8 years are detected with moderate power. During 2007-2015, ENSO records shown in Table 1 confirm 2 neutral phases in 2012/13 and 2013/14, weak and moderate El Niño in 2014/15 and 2009/10, respectively, balanced by weak and moderate La Niña in 2008/09 and 2011/12, respectively, and 2 strong La Niña occurrences in 2007/08 and 2010/11. It follows that La Niña appears to dominate over El Niño during 2007-2015 in the interannual oscillation with the recurrent interval of La Niña is found to be 2.7-3.8 years, shorter than those of El Niño. The difference in the primarily underlying periods of El Niño and La Niña suggests asymmetry in periodicity between the warm and cold phases, indicating a significant difference in the frequency of occurrence between these phases (Chen et al., 2021; Wang et al., 2023; Jia et al., 2025). This finding implies the non-stationary nature of the ENSO variability.

Another important feature from Fig. 6 is related to the power measured. The difference in intensity between the power produced by the dominant cycles of El Niño and La Niña reflects that generally El Niño is more intense than La Niña, suggesting asymmetry in intensity between ENSO phases. In support of this asymmetry, based on visual inspection on the 1975-2025 ENSO data, the strongest El Niños correspond to greater SSTAs (in magnitude) than the strongest La Niñas, consistent with earlier work (Choi et al., 2013; Ineson et al., 2021; Liang et al., 2025). SSTAs during NDJ 1982, NDJ 1997, NDJ 2015 were found to be 2.23°C, 2.39°C, 2.75°C, respectively (see Table 4), greater than those (in magnitude) for La Niña peaks during OND/NDJ/DJF from 7 cases reported in Table 5.

Depicted in Fig. 7, SSTA curves from the very strong 1982/83 and 1997/98, and extreme 2015/16 El Niño events for comparison.

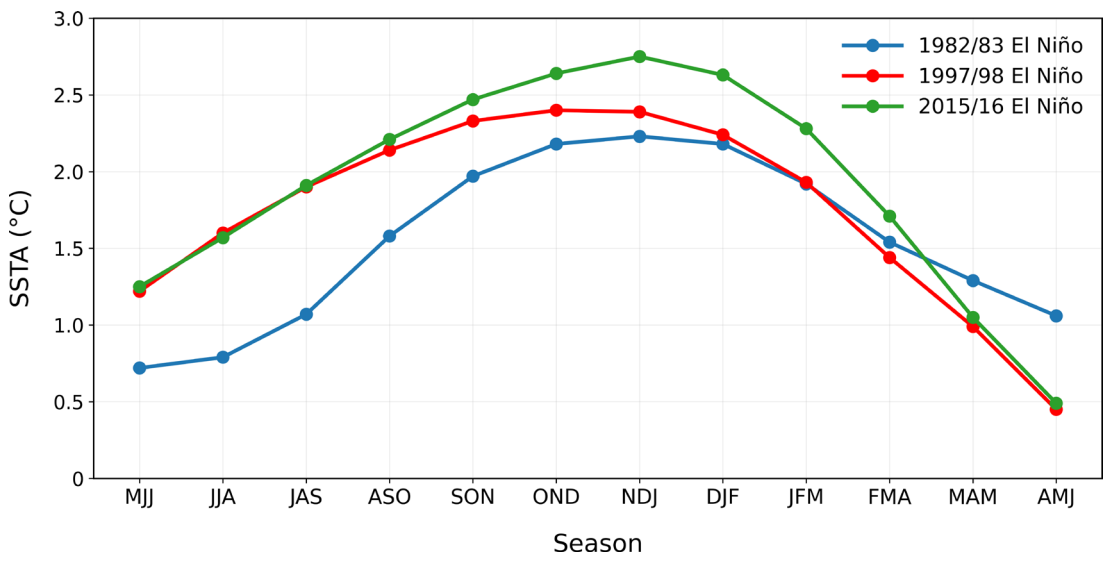

Figure 7. SSTA from the very strong 1982/83 (blue) and 1997/98 (red), and extreme 2015/16 (green) El Niño.

Table 4. SSTA during El Niño in 1982/83 and 1997/98 (very strong) and 2015/16 (extreme).

No	Season*	SSTA (°C)		
		El Niño 1982/83	El Niño 1997/98	El Niño 2015/16
1	MJJ	0.72	1.22	1.25
2	JJA	0.79	1.60	1.57
3	JAS	1.07	1.90	1.91
4	ASO	1.58	2.14	2.21
5	SON	1.97	2.33	2.47
6	OND	2.18	2.40	2.64
7	NDJ	2.23	2.39	2.75
8	DJF	2.18	2.24	2.63
9	JFM	1.92	1.93	2.28
10	FMA	1.54	1.44	1.71
11	MAM	1.29	0.99	1.05
12	AMJ	1.06	0.45	0.49

* SSTA for seasons 1-7 are taken from 1982, 1997, and 2015 while those for seasons 8-12 are obtained from 1983, 1998, and 2016.

Each curve in Fig. 7 representing the observed SSTA from different El Niño events achieves its peak during NDJ. Each El Niño episode grows to a mature phase (from JAS to NDJ) with a large amplitude, reaching its peak at about the same rate for all events. From the peak, it decays to a low SSTA where the extreme 2015/16 El Niño decays more rapidly compared to the other two, following a rapid loss of energy through oceanic heat content discharge after the growth phase (see Iwakiri and Watanabe, 2021). The SSTA patterns have demonstrated enhanced El Niño (maximum SSTA increases with time) in recent years, indicating a role of sustained warming in the tropical Pacific (see Cai et al., 2018). Using different datasets and methodologies but encompassing the same major El Niño in 1982/1983, 1997/1998, and 2015/2016, Ariska et al. (2024) reported that Indonesian rainfall pattern is sensitive to changes in SST in the central-eastern Pacific Ocean (measured by the ONI) and the western-eastern Indian Ocean (measured by the IOD) and that SST variations in the central equatorial Pacific could alter Indonesian rainfall, supported by a match between El Niño and rainfall patterns.

For comparison, the strong modes of La Niña in 1988/89, 1999/2000, 2007/08, and 2010/11 were observed with SSTAs during NDJ 1988, NDJ 1999, NDJ 2007, and NDJ 2010 measured to be −1.85°C, −1.65°C, −1.60°C, and −1.54°C, respectively, as provided in Table 5. The moderate triple-dip La Niña during 2020-2022 occured with a low SSTA of −1.20°C during NDJ 2020 and dropped to lower anomalous SST of −0.87°C during NDJ 2021 and −0.71°C during NDJ 2022. It follows that El Niño peaks are generally stronger than those of La Niña. In other words, the SSTAs in the tropical Pacific during El Niño are larger (in magnitude) than those during La Niña (see Tables 4 and 5 for comparison). The most intense El Niño is stronger than the most intense La Niña (see Figs. 7 and 8 for comparison). In the last 50 years, there has been a positive trend in the warm phase of ENSO (El Niño) to intensify, implying for

Table 5. SSTA during La Niña in 1988/89, 1999/2000, 2007/08, and 2010/11 (strong) and 2020/21, 2021/22, and 2022/23 (moderate).

No	Season*	SSTA (°C)						
		La Niña 1988/89	La Niña 1999/2000	La Niña 2007/08	La Niña 2010/11	La Niña 2020/21	La Niña 2021/22	La Niña 2022/23
1	MJJ	−1.30	−1.04	−0.47	−0.66	−0.23	−0.30	−0.78
2	JJA	−1.30	−1.10	−0.56	−1.05	−0.36	−0.35	−0.76
3	JAS	−1.11	−1.11	−0.81	−1.35	−0.53	−0.45	−0.87
4	ASO	−1.19	−1.16	−1.07	−1.56	−0.85	−0.63	−0.97
5	SON	−1.48	−1.26	−1.34	−1.64	−1.12	−0.76	−0.94
6	OND	−1.80	−1.46	−1.50	−1.64	−1.20	−0.91	−0.85
7	NDJ	−1.85	−1.65	−1.60	−1.54	−1.08	−0.87	−0.71
8	DJF	−1.69	−1.66	−1.64	−1.31	−0.91	−0.82	−0.54
9	JFM	−1.43	−1.41	−1.52	−1.04	−0.79	−0.79	−0.29
10	FMA	−1.08	−1.07	−1.29	−0.80	−0.71	−0.86	−0.02
11	MAM	−0.83	−0.81	−1.01	−0.62	−0.55	−0.95	0.27
12	AMJ	−0.58	−0.71	−0.84	−0.46	−0.39	−0.90	0.57

* SSTA for seasons 1-7 are taken from 1988, 1999, 2007, 2010, 2020, 2021, and 2022 whereas those for seasons 8-12 are obtained from 1989, 2000, 2008, 2011, 2021, 2022, and 2023.

ENSO asymmetry in amplitude hence intensity, as reported by earlier work (Choi et al., 2013; Geng et al., 2019; Chen et al., 2021; Ineson et al., 2021; Jia et al., 2025; Liang et al., 2025).

We provide in Fig. 8 separate graphs of SSTA from the strong 1988/89, 1999/2000, 2007/08, and 2010/11 La Niña and the moderate triple-dip La Niña between 2020-2022 for comparison. Different from El Niño, La Niña achieves the lowest SSTA during OND/NDJ/DJF. From the onset, La Niña grows to a mature phase with a large amplitude in magnitude (a positive value), reaching its lowest intensity at about the same rate (except for the 2022/23 period). The 2020/21 La Niña persisted into the second and third years (Geng et al., 2023), supporting a longer duration of the corresponding La Niña cycle, leading to the triple-dip La Niña of 2020-2022. However, the SSTA for La Niña reveals no clear pattern of the anomalies with respect to time.

The ENSO variability in terms of asymmetric periodicity and intensity between the El Niño and La Niña phases is believed to have deep impacts on a changing climate at regional and global scales. The asymmetry in periodicity possibly results from the fact that ENSO duration is likely controlled by decay rates, where it is relatively slow for La Niña than El Niño. Whilst, the amplitude asymmetry is related to non-linear atmospheric and oceanic processes as positive feedback in the highly complex atmosphere-ocean interaction. These are beyond the scope of this study. Thorough reviews on the characteristics, mechanisms, and implications of the ENSO asymmetry can be examined in Liang et al. (2025). In addition to major ENSO interannual time-scales of 3-8 years (Okumura and Deser, 2010; Chen et al., 2024), the FFT and CWT identify ENSO fluctuations at time-scales of equal to or longer than 10 years,

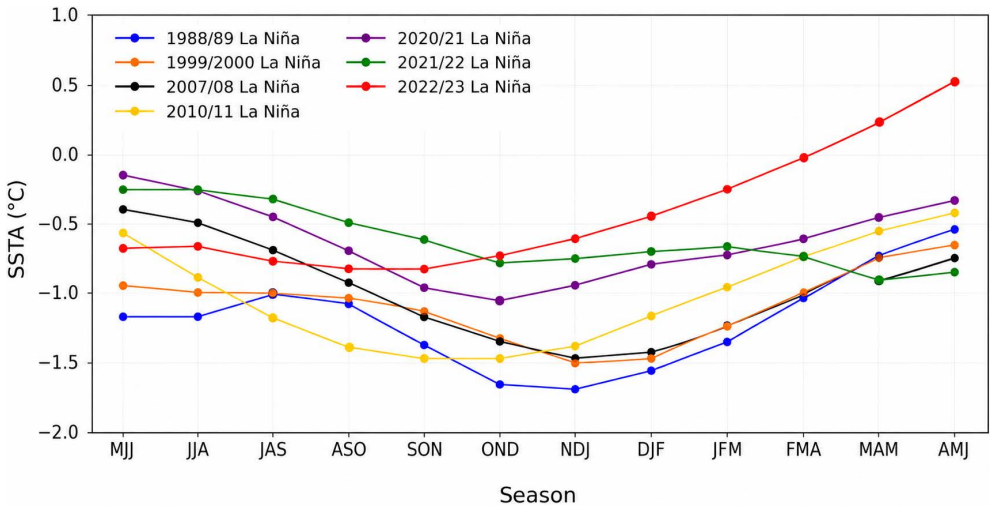

Figure 8. SSTA from the strong 1988/89 (blue), 1999/2000 (brown), 2007/08 (black), and 2010/11 (yellow), and the moderate triple-dip 2020/21 (violet), 2021/22 (green), and 2022/23 (red) La Niña.

suggesting the relative significance of decadal variations to the non-stationary nature of ENSO characteristics (Sullivan et al., 2016; Chen et al., 2024). In short, both advanced time-frequency methods are considered successful to solve the ENSO asymmetry in periodicity and intensity.

3.3 Impacts of ENSO asymmetry on rainfall variability

To obtain further information on the relationship between ENSO and rainfall patterns, in particular the impacts of ENSO asymmetric behaviours in terms of the asymmetry in periodicity and intensity on rainfall variability over Indonesia, we apply the CWT technique to high-resolution rainfall datasets of CRU-TS 4.09 between 1975-2024 and provide the results in Fig. 9.

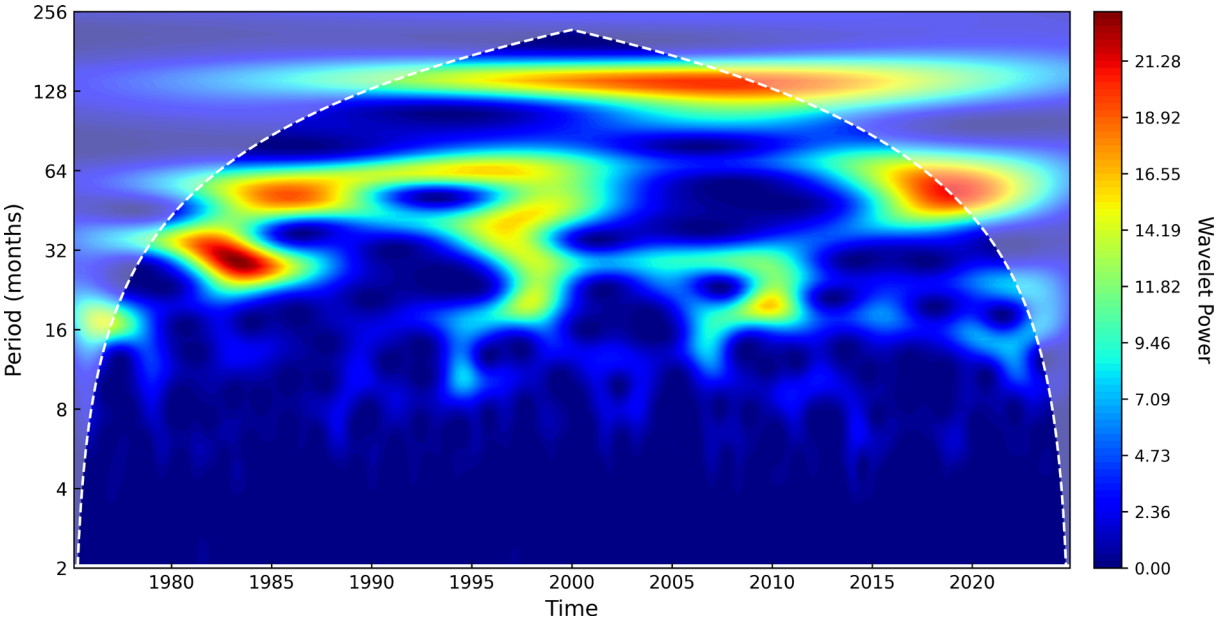

Figure 9. The results of the CWT on rainfall datasets with the COI is seen as a curved white dashed-line, covering regions within which interpretation is believed to be true. The wavelet shows the nature of rainfall anomalies, which vary with time of observation (in years) and period of oscillation (in months).

It is clear by visual inspection at glance that in general features seen in Fig. 6 are similar to those seen in Fig. 9, suggesting the impacts of ENSO on annual rainfall variability over Indonesia. However, several concentrated areas of relatively high energy level are detected within the COI, as depicted in Fig. 9. The highest level is associated with a period of 24-36 months equivalent to 2.0-3.0 years between 1981-1986, consistent with the early finding of the dominant time-scale of Indonesian rainfall variability during 1961-1990 (Hamada et al., 2002). It is followed by slightly lesser power with a period of 48-62 months equivalent to 4.0-5.2 years between 1983-1988. Indeed, the supremely strong 1987/88 and very strong 1982/83 El Niño events characterised 1981-1988 (Chen et al., 2024), suggesting that large amounts of mean annual rainfall deficits across the country during these years are induced by the strong influence of El Niño (Ariska et al., 2024). Droughts during the dry seasons (JJA and SON) in 1982/83 and 1987/88 throughout the country were observed with the co-occurrence of positive Indian Ocean Dipole (IOD) and El Niño (Hamada et al., 2012; Amirudin et al., 2020; Kurniadi et al., 2021). Similar dry conditions occurred with significantly altered rainfall patterns during the 1997/98 and 2015/16 El Niño events (Ariska et al., 2024).

For a long period of 18-72 months equivalent to 1.5-6.0 years between 1995-1999, a weaker level but remaining in moderate power exists with various reasons; one of which is that the very strong 1997/98 El Niño is balanced by the moderate 1995/96 and strong 1998/99 La Niña events, leaving this period with no dominance of either El Niño or La Niña hence no significant changes in mean rainfall amounts recorded in Indonesia. The apparent high power with a period of 48-76 months equivalent to 4.0-6.3 years after 2015 is attributable to the extreme 2015/16 El Niño (Paek et al., 2017; Lestari et al., 2018) with the highest record of SSTA reported to be 2.75°C during NDJ 2015, causing severely prolonged droughts throughout the country. A relatively small porsion of an area within the COI with moderate power is seen to occur between 2009-2012 in a period of 20-24 months equivalent to 1.7-2.0 years, corresponding to the strong La Niña in 2010/11. The results in these periods are somewhat ambiguous as they are interfered by another possible cause regarding oscillation at time-scales longer than 96 months (see Fig. 9).

Different from Fig. 6, Fig. 9 reveals a remarkable level of power related to relatively strong decadal oscillation at time-scales of 10.0-13.3 years (120-150 months), extending from 1998 to 2010 within the COI. It follows that rainfall patterns over Indonesia are likely complex, not only coupled with the short-term, interannual variations of the ENSO but also affected by influential factors other than El Niño and La Niña episodes, such as the IOD in particular at interannual modes (Lestari et al., 2018; Amirudin et al., 2020; Kurniadi et al., 2021; Ariska et al., 2024), and Madden-Julian Oscillation (MJO) (see Ratri et al., 2021) and Pacific Decadal Oscillation (PDO) (see Lee, 2015) in the long-term significance, affecting Indonesian rainfall variability at decadal time-scales.

As shown in Fig. 9, we find the complexity of Indonesian rainfall anomalies revealing 3 distinct time-intervals with considerable levels of wavelet power at periods between 2.0-3.0 years, 4.0-5.2 years, and 10.0-13.3 years. Among these time-scales, the mode of ~4-5 years is likely relevant to ENSO (El Niño) having the dominant period (also known as the recurrent interval) of 3.7-5.2 years, within the range of 3-8 years for interannual fluctuation (Okumura and Deser, 2010; Chen et al., 2024). This suggests that rainfall variability across Indonesia is driven by the ENSO phases at a primary mode of interannual variations, while remaining affected by climate variability at various time-scales, either shorter or longer than the primary mode. With a shorter dominant period of La Niña (2.7-3.8 years for the recurrent interval) than El Niño, rainfall in Indonesia is expected to occur frequently, thereby increasing the potency of rainfall extreme that may lead to floods and landslides in prone regions. With a greater intensity of the power during El Niño events than La Niña events, atmospheric conditions over Indonesia are drier, along with significantly reduced amounts of rainfall, hence increasing the possibility of significant rainfall deficits that may lead to droughts and forest fires. In short, the impacts of the ENSO asymmetry in periodicity and intensity on Indonesian rainfall variability are, with the corresponding anomalies are either deficit or surplus in amounts, related to possible hydrometeorological hazards in the future.

To complete discussions, we provide in Fig. 10 annual precipitation amounts in Indonesia between 1975-2024 (rainfall data for 2025 are unavailable), which provides further insight into the impacts of ENSO asymmetry on rainfall variability. Such long observations allow us to have a long-term trend, whether there is a clear pattern of reduced (increased) precipitation during El Niño (La Niña). The black dashed-line is the mean annual precipitation (2778 mm). Starting from late 1990s afterwards, the net amount of precipitation anomaly (measured from the mean annual precipitation) is positive since the blue curve covers more areas above the black dashed-line, implying more frequent La Niña than El Niño (bringing more rainfall to Indonesia with significant departures from the mean). Double triple-dip La Niña events in 1998-2000 and 2020-2022 indicate a trend in multi-year La Niña, leading to longer duration of La Niña. Differences in frequency of occurrence and a life-cycle between El Niño and La Niña reflect ENSO asymmetry in periodicity.

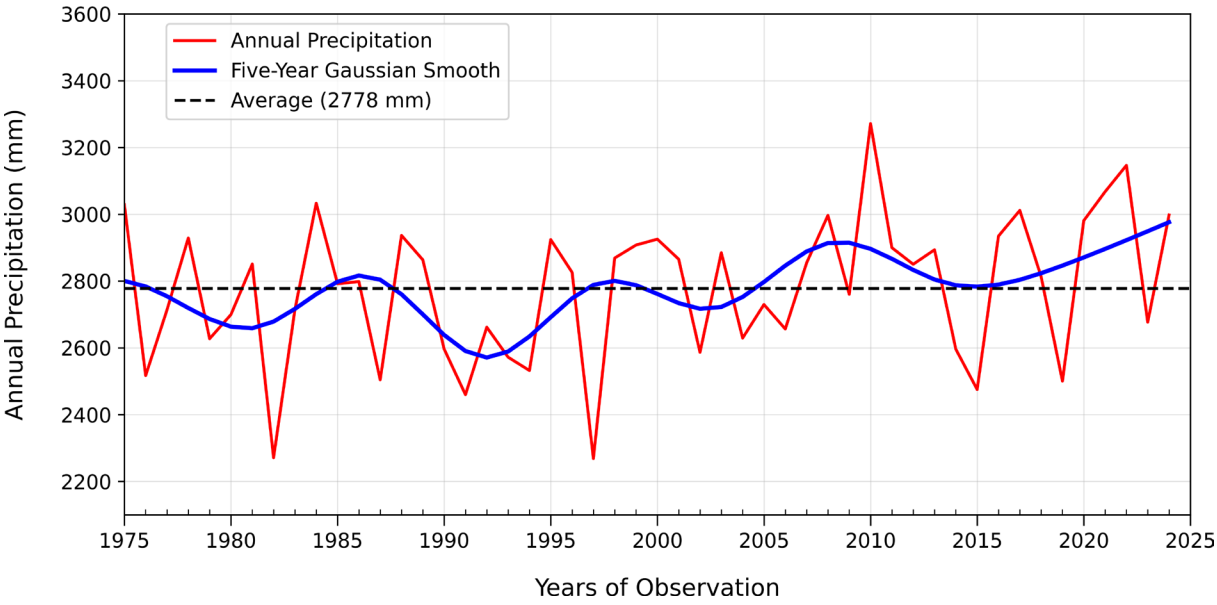

Figure 10. Rainfall variability over Indonesia between 1975-2024, where annual precipitation is represented by the red curve, the 5-year Gaussian smooth is shown by the blue curve, and the average precipitation is represented by the black dashed-line.

Figure 10 describes the 1982/83 El Niño to be similar to the 1997/98 El Niño in terms of annual precipitation. The annual precipitation of both was much reduced from the mean value to 2271 mm and 2268 mm, respectively. Drier conditions leading to prolonged droughts were reported to strike the majority of Indonesian territory during these two severe events (Kirono et al., 1999) and another major El Niño occurred in 2015/16 (Lestari et al., 2018). The extreme 2015/16 El Niño came with a lesser amount of reduction, where the precipitation was observed to be 2475 mm. With an approximately 300 mm reduction in the precipitation compared with the other severe El Niño, it turned out to cause less destruction.

Amongst La Niña events between 1975-2025, the most notable ones were those in 2010/11 with a strong mode of 3271 mm and the 2020-2022 triple-dip La Niña with moderate intensity of 3146 mm (see Fig. 10). It follows that the largest increase in the precipitation is detected to be 493 mm for the 2010/11 La Niña and the second largest is observed to be 368 mm, attributable to the 2020-2022 triple-dip case. Rainfall intensities in other La Niña events during observations are lower than these episodes, suggesting that the increased amount of precipitation during La Niña is smaller than its reduced amount during El Niño, thereby reflecting ENSO asymmetry in intensity.

In terms of geospatial variability of Indonesian rainfall, the MJO is found to control differences in amplitude of rainfall patterns between the western and eastern regions of Indonesia (Hidayat, 2016). Further, a stronger impact of the ENSO is found to accumulate in the northern and eastern regions of Indonesia, but the IOD is observed to influence more on the southern and western sides (Kurniadi et al., 2021). The differential impacts on the patterns of anomalous rainfall in Indonesia are influenced by a strongly coupled ocean-atmosphere system, which induces regional changes in oceanic temperatures and atmospheric circulations (Amirudin et al., 2020). But these topics are beyond the scope of the present study, which discusses temporal variability of the large-scale rainfall anomalies across Indonesia as a whole. Given the large-scale geospatial variability of different rainfall regimes hence patterns across the country, this spatial aggregation may help resolve significant regional differences in ENSO impacts.

In summary, Indonesian precipitation rates relate to ENSO asymmetry in periodicity and intensity. Given that the role of ENSO phases in modulating climate is of significance, its asymmetric behaviour is essential. More work is required to better understand the ENSO asymmetry and its close relation to rainfall variability over Indonesia. In particular, Indonesia is a country with a widely spanning longitude-border from west to east, making it diverse mainly owing to large-scale differences in geographical provinces, topographical lanscapes, and monsoonal winds. Examination of Indonesian climate through routine and accurate rainfall monitoring may be best performed using assessment of a sub-national scale based on distinct climatic zones for further work.

4. Conclusions

We have investigated ENSO variability and its asymmetric behaviours in terms of periodicity and intensity of the ENSO phases (El Niño and La Niña) in Indonesia between 1975-2025 using particularly the ONI time-series from the Niño 3.4 region in the equatorial Pacific and the corresponding SOI time-series. We have also examined the impacts of the ENSO asymmetry on Indonesian rainfall variability. Both statistical and technical approaches, including the Pearson and lagged correlation analyses, and the FFT and wavelet techniques, are together used to characterise the non-stationary nature of the ENSO variability. Statistical tools reveal that the ONI and the SOI are strongly correlated within the Niño 3.4 across observational years with the Pearson coefficient of –0.76, suggesting that the indices are good indicators for El Niño and La Niña, in line with earlier studies, while being correlated with rainfall patterns over Indonesia at only moderate modes of –0.63 and 0.59, respectively. With p-values from all correlations are below a cut-off of 0.05, these variables are proved to be statistically significant. The strong impacts of El Niño occur during dry season in JJA and SON, consistent with previous studies. Time-lag analysis shows that significant rainfall anomalies lead by 3 months over the peaks of El Niño in NDJ.

Technical tools include time-frequency methods, namely the FFT and CWT analyses. The FFT shows two modes of ENSO oscillation: the short-term (shorter than 8 years) interannual and the long-term (longer than 10 years) decadal variations, implying the non-stationary (time-dependent) nature of ENSO variability. Using the CWT, a more detailed technique, we find that the recurrent intervals of El Niño and La Niña episodes are lying between 3.7-5.2 years and 2.7-3.8 years, respectively, falling within the range of 3.1-5.5 years estimated for the main mode of ENSO cycles at interannual variability. This technique also reveals asymmetric behaviours in terms of periodicity and intensity of both El Niño and La Niña. With a shorter recurrent interval, La Niña appears more frequently than El Niño, leading to a greater possibility of hydrological hazards, such as floods and landslides to take place. Whilst, with generally a higher intensity, particularly during strong El Niño events, El Niño tends to be more intense with drier atmospheric conditions that may lead to a greater possibility of meteorological hazards, such as droughts and forest fires to occur. This is of significance to Indonesia possibly affected by the potency of frequent climate-related hazards, which bring possible extreme weather with severe impacts in the future.

The authors' statement. The authors declare that no financial support was received during the completion of the work and no conflict of interest regarding this work.

Data availability. For clarity, definitions of ONI and SOI characterising the warm (El Niño) and cold (La Niña) ENSO phases can be seen at https://www.ncei.noaa.gov/access/monitoring/enso. Seasonal and monthly data for ONI collected from field measurements of SST anomaly (SSTA) in the Niño 3.4 region were made available by Climate Prediction Center (CPC), NCEP-NOAA available at https://www.cpc.ncep.noaa.gov/data/indices. Data for seasonal ONI variations were taken from https://www.cpc.ncep.noaa.gov/data/indices/oni.ascii.txt and monthtly variations from https://www.cpc.ncep.noaa.gov/products/analysis_monitoring/ensostuff/detrend.nino34.ascii.txt. Data for SOI were taken from https://www.cpc.ncep.noaa.gov/data/indices/soi.3m.txt. Data for rainfall variability in Indonesia were provided by Climate Change Knowledge Portal (CCKP) by World Bank Group (WBG) available at https://climateknowledgeportal.worldbank.org/country/indonesia/climate-data-historical based on CRU-TS 4.08 (annual rainfall) and https://crudata.uea.ac.uk/cru/data/hrg/ based on CRU-TS 4.09 (monthly rainfall).

Acknowledgements. The authors would firmly like to thank NCEP-NOAA, the US government for the ONI and SOI data used in this study. Special thanks go to the WBG for free accessibility in Indonesian rainfall variability. This study has benefited constructive comments and suggestions from anonymous reviewers during reviews.

References

Aldrian, E. and R. D. Susanto (2003). Identification of three dominant rainfall regions within Indonesia and their relationship to sea surface temperature, Int. J. Climatol., 23, 12, 1435-1452, doi:10.1002/joc.950.

Aldrian, E., L. Dümenil Gates and F. H. Widodo (2007). Seasonal variability of Indonesian rainfall in ECHAM4 simulations and in the reanalyses: The role of ENSO, Theor. Appl. Climatol., 87, 41-59, doi:10.1007/s00704-006-0218-8.

Amirudin, A. A., E. Salimun, F. Tangang, L. Juneng et al. (2020). Differential influences of teleconnections from the Indian and Pacific Oceans on rainfall variability in Southeast Asia, Atmosphere, 11, 9, 886, doi:10.3390/atmos11090886.

An, S. I. and J. W. Kim (2017). Role of nonlinear ocean dynamic response to wind on the asymmetrical transition of El Niño and La Niña, Geophys. Res. Lett., 44, 1, 393-400, doi:10.1002/2016GL071971.

Ariska, M., Suhadi, Supari, M. Irfan et al. (2024). Spatio-temporal variations of Indonesian rainfall and their links to Indo-Pacific modes, Atmosphere, 15, 9, 1036, doi:10.3390/atmos15091036.

Ayarzagüena, B., S. Ineson, N. J. Dunstone, M. P. Baldwin et al. (2018). Intraseasonal effects of El Niño-Southern Oscillation on North Atlantic climate, J. Clim., 31, 21, 8861-8873, doi:10.1175/JCLI-D-18-0097.1.

Barnston, A. G., M. Chelliah and S. B. Goldenberg (1997). Documentation of a highly ENSO-related SST region in the equatorial Pacific: Research note, Atmos. Ocean, 35, 3, 367-383, doi:10.1080/07055900.1997.9649597.

Bjerknes, J. (1969). Atmospheric teleconnections from the equatorial Pacific, Monthly Weather Rev., 97, 3, 163-172, doi:10.1175/1520-0493(1969)097<0163:ATFTEP>2.3.CO;2.

Bunge, L. and A. J. Clarke (2009). A verified estimation of the El Niño index Niño-3.4 since 1877, J. Clim., 22, 14, 3979-3992, doi:10.1175/2009JCLI2724.1.

Cai, W., G. Wang, B. Dewitte, L. Wu et al. (2018). Increased variability of eastern Pacific El Niño under greenhouse warming, Nature, 564, 201-206, doi:10.1038/s41586-018-0776-9.

Chen, H., J. Shi, Y. Jin, T. Geng et al. (2021). Warm and cold episodes in western Pacific warm pool and their linkage with ENSO asymmetry and diversity, J. Geophys. Res. Oceans, 126, 12, e2021JC017287, doi:10.1029/2021JC017287.

Chen, Y., C. Zhao and H. Zhi (2024). Analysis of ENSO event intensity changes and time-frequency characteristic since 1875, Atmosphere, 15, 1428, doi:10.3390/atmos15121428.

Choi, K. Y., G. A. Vecchi and A. T. Wittenberg (2013). ENSO transition, duration, and amplitude asymmetries: Role of the nonlinear wind stress coupling in a conceptual model, J. Clim., 26, 23, 9462-9476, doi:10.1175/JCLI-D-13-00045.1.

Crockett, R. (2019). Using the FFT to identify periodic features in time-series, in A primer on Fourier Analysis for the Geosciences, 69-91, Cambridge, Cambridge Uni. Press, UK, doi:10.1017/9781316543818.007.

Ehsan, M. A., M. L. L'Heureux, M. K. Tippett, A. W. Robertson et al. (2024). Real-time ENSO forecast skill evaluated over the last two decades, with focus on the onset of ENSO events, Clim. Atmos. Sci., 7, 301, doi:10.1038/s41612-024-00845-5.

Fan, H., C. Wang and S. Yang (2023). Asymmetry between positive and negative phases of the Pacific Meridional Mode: A contributor to ENSO transition complexity, Geophys. Res. Lett., 50, 14, e2023GL104000, doi:10.1029/2023GL104000.

Feldstein, S. B. and C. L. E. Franzke (2017). Atmospheric Teleconnection Patterns, in Nonlinear and Stochastic Climate Dynamics C. L. E. Franzke and T. J. O'Kane (Eds.), Cambridge University Press, Cambridge, 54-104, doi:10.1017/9781316339251.004.

Freund, M. B., J. R. Brown, A. G. Marshall, C. R. Tozer et al. (2024). Interannual ENSO diversity, transitions, and projected changes in observations and climate models, Environ. Res. Lett., 19, 11, 114005, doi:10.1088/1748-9326/ad78db.

Geng, T., W. Cai, L. Wu and Y. Yang (2019). Atmospheric convection dominates genesis of ENSO asymmetry, Geophys. Res. Lett., 46, 14, 8387-8396, doi:10.1029/2019GL083213.

Geng, T., F. Jia, W. Cai, L. Wu et al. (2023). Increased occurrences of consecutive La Niña events under global warming, Nature, 619, 7971, 774-781, doi:10.1038/s41586-023-06236-9.

Ghil, M., M. R. Allen, M. D. Dettinger, K. Ide et al. (2002). Advanced spectral methods for climatic time series, Rev. Geophys., 40, 1, 1003, doi:10.1029/2000RG000092.

Glantz, M. H. and I. J. Ramirez (2020). Reviewing the Oceanic Niño Index (ONI) to enhance societal readiness for El Niño's impacts, Int. J. Disaster Risk Sci., 11, 394-403, doi:10.1007/s13753-020-00275-w.

Glantz, M. H. and I. J. Ramírez (2025). Enhancing societal value of early warning early action and anticipatory action frameworks using NOAA's Oceanic Niño Index, Int. J. Disaster Risk Sci., 16, 171-181, doi:10.1007/s13753-025-00625-6.

Greenland, S., S. J. Senn, K. J. Rothman, J. B. Carlin et al. (2016). Statistical tests, *P* values, confidence intervals, and power: a guide to misinterpretations, Eur. J. Epidemiol., 31, 337-350, doi:10.1007/s10654-016-0149-3.

Hamada, J. I., M. D. Yamanaka, J. Matsumoto, S. Fukao et al. (2002). Spatial and temporal variations of the rainy season over Indonesia and their link to ENSO, J. Meteorol. Soc. Jpn., Ser II, 80, 2, 85-310, doi:10.2151/jmsj.80.285.

Hamada, J. I., S. Mori, H. Kubota, M. D. Yamanaka et al. (2012). Interannual rainfall variability over northwestern Jawa and its relation to the Indian Ocean Dipole and El Niño-Southern Oscillation Events, SOLA, 8, 69-72, doi:10.2151/sola.2012-018.

Hendon, H. H. (2003). Indonesian rainfall variability: Impacts of ENSO and local air-sea interaction, J. Clim., 16, 11, 1775-1790, doi:10.1175/1520-0442(2003)016<1775:IRVIOE>2.0.CO;2.

Hidayat, R. (2017). Modulation of Indonesian rainfall variability by the Madden-Julian Oscillation, Procedia Environ. Sci., 33, 167-177, doi:10.1016/j.proenv.2016.03.067.

Huang, B., P. W. Thorne, V. F. Banzon, T. Boyer et al. (2017). Extended Reconstructed Sea Surface Temperature, Version 5 (ERSSTv5): Upgrades, validations, and intercomparisons, J. Clim., 30, 20, 8179-8205, doi:10.1175/JCLI-D-16-0836.1.

Ineson, S., N. J. Dunstone, H. L. Ren, R. Renshaw et al. (2021). ENSO amplitude asymmetry in Met Office Hadley Centre Climate Models, Front. Clim., 3, 789869, doi:10.3389/fclim.2021.789869.

Iwakiri, T. and M. Watanabe (2021). Mechanisms linking multi-year La Niña with preceding strong El Niño, Sci. Rep., 11, 1, 17465, doi:10.1038/s41598-021-96056-6.

Jia, F., W. Cai, T. Geng, B. Gan et al. (2025). Transition from multi-year La Niña to strong El Niño rare but increased under global warming, Sci. Bull., 70, 5, 756-764, doi:10.1016/j.scib.2024.12.034.

Julian, P. R. and R. M. Chervin (1978). A study of the southern oscillation and Walker circulation phenomenon, Monthly Weather Rev., 106, 10, 1433-1451, doi:10.1175/1520-0493(1978)106<1433:ASOTSO>2.0.CO;2.

Kayano, M. T., W. L. Cerón, R. V. Andreoli, R. A. F. Souza et al. (2021). El Niño-Southern Oscillation and Indian Ocean Dipole modes: Their effects on south American rainfall during austral spring, Atmosphere, 12, 11, 1437, doi:10.3390/atmos12111437.

Kirono, D. G. C., N. J. Nigel and J. L. McBride (1999). Documenting Indonesian rainfall in the 1997/1998 El Niño event, Phys. Geogr., 20, 5, 422-435, doi:10.1080/02723646.1999.10642687.

Kralj, L., M. Hultman and H. Lenasi (2024). Wavelet analysis and the Cone of Influence: Does the Cone of Influence impact wavelet analysis results?, Appl. Sci., 14, 24, 11736, doi:10.3390/app142411736.

Kurniadi, A., E. Weller, S. K. Min and M. G. Seong (2021). Independent ENSO and IOD impacts on rainfall extremes over Indonesia, Int. J. Climatol., 41, 6, 3640-3656, doi:10.1002/joc.7040.

Le, T. and D. H. Bae (2019). Causal links on interannual timescale between ENSO and the IOD in CMIP5 future simulations, Geophys. Res. Lett., 46, 5, 2820-2828, doi:10.1029/2018GL081633.

Lee, H. S. (2015). General rainfall patterns in Indonesia and the potential impacts of local seas on rainfall intensity, Water, 7, 4, 1751-1768, doi:10.3390/w7041751.

L'Heureux, M. L., M. K. Tippett, M. C. Wheeler, H. Nguyen et al. (2024). A relative sea surface temperature index for classifying ENSO events in a changing climate, J. Clim., 37, 4, 1197-1211, doi:10.1175/JCLI-D-23-0406.1.

Lestari, D. O., E. Sutriyono, Sabaruddin and I. Iskandar (2018). Severe drought event in Indonesia following 2015/16 El Niño/positive Indian Dipole events, IOP J. Phys. Conf. Ser., 1011, 012040, doi:10.1088/1742-6596/1011/1/012040.

Li, X., Z. Z. Hu, Y. H. Tseng, Y. Liu et al. (2022). A historical perspective of the La Niña event in 2020/2021, J. Geophys. Res. Atmos., 127, 7, e2021JD035546, doi:10.1029/2021JD035546.

Li, A., Y. Zhang, M. Hong, J. Shi et al. (2023). Relative importance of ENSO and IOD on interannual variability of Indonesian Throughflow transport, Front. Mar. Sci., 10, 1182255, doi:10.3389/fmars.2023.1182255.

Li, X., J. Y. Yu and R. Ding (2024). El Niño-La Niña asymmetries in the changes of ENSO complexities and dynamics since 1990, Geophys. Res. Lett., 51, 6, e2023GL106395, doi:10.1029/2023GL106395.

Liang, J., D. Z. Sun., B. Jin, Y. Yang et al. (2025). The asymmetry of the El Niño-Southern Oscillation: Characteristics, mechanisms, and implications for a changing climate, Atmoshere, 16, 9, 1071, doi:10.3390/atmos16091071.

Liu, T., X. Song, Y. Tang, Z. Sen et al. (2022). ENSO predictability over the past 137 years based on a CESM ensemble prediction system, J. Clim., 35, 2, 763-777, doi:10.1175/JCLI-D-21-0450.1.

Masood, M. U., S. Haider, M. Rashid, M. U. K. Lodhi et al. (2023). The effect of the El Nino Southern Oscillation on precipitation extremes in the Hindu Kush mountains range, Water, 15, 24, 4311, doi:10.3390/w15244311.

McPhaden, M. J. (2015). Playing hide and seek with El Niño, Nat. Clim. Change, 5, 9, 791-795, doi:10.1038/nclimate2775.

McPhaden, M. J., A. Santoso and W. Cai (Eds.) (2020). El Niño-Southern Oscillation in a changing climate, Geophys. Monogr. Ser., 253, Amer. Geophys. Union, doi:10.1002/9781119548164.

Molteni, F. and A. Brookshaw (2023). Early-and late-winter ENSO teleconnections to the Euro-Atlantic region in state-of-the-art seasonal forecasting systems, Clim. Dyn., 61, 5-6, 2673-2692, doi:10.1007/s00382-023-06698-7.

Okumura, Y. M. and C. Deser (2010). Asymmetry in the duration of El Niño and La Niña, J. Clim., 23, 21, 5826-5843, doi:10.1175/2010JCLI3592.1.

Paek, H., J. Y. Yu and C. Qian (2017). Why were the 2015/2016 and 1997/1998 extreme El Niños different?, Geophys. Res. Lett., 44, 4, 1848-1856, doi:10.1002/2016GL071515.

Parra, R. R. T., D. F. B. Usta, L. J. O Díaz and M. P. Moreno-Ardila (2024). Eastern tropical Pacific atmospheric and oceanic projected changes based on CMIP6 models, Prog. Oceanogr., 229, 2, 103362, doi:10.1016/j.pocean.2024.103362.

Ratri, D. N., K. Whan and M. Schmeits (2021). Calibration of ECMWF seasonal ensemble precipitation reforecasts in Java (Indonesia) using bias-corrected precipitation and climate indices, Weather Forecasting, 36, 4, 1375-1386, doi:10.1175/WAF-D-20-0124.1.

Santos, C. A. G., D. C. dos Santos, R. M. B. Neto, G. de Oliveira et al. (2024). Analyzing the impact of ocean-atmosphere teleconnections on rainfall variability in the Brazilian Legal Amazon via the Rainfall Anomaly Index (RAI), Atmos. Res., 307, 1, 107483, doi:10.1016/j.atmosres.2024.107483.

Santoso, A., M. H. England, J. B. Kajtar and W. Cai (2022). Indonesian Throughflow variability and linkage to ENSO and IOD in an ensemble of CMIP5 models, J. Clim., 35, 10, 3161, doi:10.1175/JCLI-D-21-0485.1.

Sayol, J. M., L. M. Vásquez, J. L. Valencia, J. R. Linero-Cueto et al. (2022). Extension and application of an observation-based local climate index aimed to anticipate the impact of El Niño-Southern Oscillation events on Colombia, Int. J. Climatol., 42, 11, 5403-5429, doi:10.1002/joc.7540.

Schober, P., C. Boer and L. A. Schwarte (2018). Correlation coefficients: Appropriate use and interpretation, Anesthesia and Analgesia, 126, 5, 1763-1768, doi:10.1213/ANE.0000000000002864.

Setyaningrum, N., E. Trihatmoko, P. Sofan, A. G. Suhadha et al. (2026). SBAS-InSAR monitoring and time-lag correlation analysis of peatland subsidence in Central Kalimantan, Indonesia, Can. J. Remote Sens., 52, 1, 663665, doi:10.1080/07038992.2026.2663665.

Sullivan, A., J. J. Luo, A. C. Hirst, D. Bi et al. (2016). Robust contribution of decadal anomalies to the frequency of central-Pacific El Niño, Sci. Rep., 6, 38540, 1-7, doi:10.1038/srep38540.

Tamaddun, K. A., A. Kalra and S. Ahmad (2017). Wavelet analyses of western us streamflow with ENSO and PDO, J. Water Clim. Chang., 8, 1, 26-39, doi:10.2166/wcc.2016.162.

Timmermann, A., S. I. An, J. S. Kug, F. F. Jin et al. (2018). El Niño Southern Oscillation complexity, Nature, 559, 7715, 535-545, doi:10.1038/s41586-018-0252-6.

Torres, R. R., E. Giraldo, C. Muñoz, A. Caicedo et al. (2023). Seasonal and El Niño-Southern Oscillation-related ocean variability in the Panama Bight, Ocean. Sci., 19, 3, 685-701, doi:10.5194/os-19-685-2023.

Walker, G. T. (1928). World weather, Quarterly J. Royal Met. Soc., 54, 226, 79-87, doi:10.1002/qj.49705422601.

Wang, B., W. Sun, C. Jin, X. Luo et al. (2023). Understanding the recent increase in multiyear La Niñas, Nat. Clim. Change, 13, 10, 1075-1081, doi:10.1038/s41558-023-01801-6.

***CORRESPONDING AUTHOR: Endah RAHMAWATI**,
The State University of Surabaya, Physics Department, Surabaya, Indonesia
e-mail: endahrahmawati@unesa.ac.id
© 2026 the Author(s).
Open Access. This article is licensed under a Creative Commons Attribution 4.0 International License